Superconductivity in $La_4Ni_3O_{10}$ under pressure

Chen Lu [1,*] Zhiming Pan,[2,*] Fan Yang,[3,†] and Congjun Wu [4,5,6,7,‡]

[1]*School of Physics, Hangzhou Normal University, Hangzhou 311121, China*

[2]*Department of Physics, Xiamen University, Xiamen 361005, China*

[3]*School of Physics, Beijing Institute of Technology, Beijing 100081, China*

[4]*New Cornerstone Science Laboratory, Department of Physics, School of Science, Westlake University, Hangzhou 310024, Zhejiang, China*

[5]*Institute for Theoretical Sciences, Westlake University, Hangzhou 310024, Zhejiang, China*

[6]*Key Laboratory for Quantum Materials of Zhejiang Province, School of Science, Westlake University, Hangzhou 310024, Zhejiang, China*

[7]*Institute of Natural Sciences, Westlake Institute for Advanced Study, Hangzhou 310024, Zhejiang, China*

(Received 6 February 2025; revised 7 April 2025; accepted 11 April 2025; published 22 April 2025)

The discovery of superconductivity (SC) in the trilayer nickelate compound $La_4Ni_3O_{10}$ under pressure has generated significant interest. In this work, we propose a trilayer two E_g-orbital t-$J_\parallel$-$J_\perp$ model to investigate the microscopic origin of SC in this system. In the strong-coupling regime, each layer is governed by a t-$J_\parallel$ model with intralayer antiferromagnetic exchange $J_\parallel$, while electrons are allowed to hop between layers, interacting via interlayer exchange $J_\perp$. The inner-layer $3d_{z^2}$-orbital electrons tend to form bonding states with those in the neighboring layers, leading to redistribution of the electron densities. The numerical simulation results indicate that SC is predominantly mediated by the $3d_{z^2}$ orbital, characterized by an intralayer extended s-wave pairing in the outer layers, accompanied by an interlayer pairing with opposite sign. Furthermore, we find that electron doping enhances SC, while hole doping tends to suppress it. These findings provide new insights into the SC mechanisms of $La_4Ni_3O_{10}$ and its sensitivity to charge doping.

DOI: 10.1103/PhysRevB.111.134515

I. INTRODUCTION

The Ruddlesden-Popper phase nickelates series $La_{n+1}Ni_nO_{3n+1}$ has attracted significant attention for a long time due to its potential for hosting unconventional superconductivity (SC) [1–18]. A major breakthrough occurred with the discovery of SC in the infinite-layer $Nd_{0.8}Sr_{0.2}NiO_3$ ($n = \infty$) [19]. More recently, high-temperature SC ($T_c \approx 80$ K) was observed in $La_3Ni_2O_7$ ($n = 2$) under pressure exceeding 14 GPa [20–24], sparking further investigations. Further excitement was generated by the successful realization of SC in thin-film $La_3Ni_2O_7$ under ambient pressure, exhibiting T_c approximately 40 K [25]. Additionally, experimental evidence of SC ($T_c \approx 20$ K) under pressure in $La_4Ni_3O_{10}$ ($n = 3$) [26–28] has drawn considerable attention [29–54].

The potential SC in $La_{n+1}Ni_nO_{3n+1}$ is intricately related to the electronic properties of the NiO_2 planes, contributing from the Ni E_g orbitals. In single NiO_2 layer, the two E_g orbitals are nearly degenerate. However, in a multilayer system, interlayer hopping lifts this degeneracy by forming bonding and antibonding bands. Based on the density-functional theory (DFT) calculations [12,20,55], a bilayer two-orbital model has been proposed to explain the high-T_c SC in $La_3Ni_2O_7$ [56,57], where the bonding band of the $3d_{z^2}$ orbital is nearly fully occupied and localized. In the strong-coupling limit, the $3d_{z^2}$ orbital exhibits robust interlayer superexchange, which is transmitted to the $3d_{x^2-y^2}$ orbital under strong Hund's rule [56–61], significantly enhancing the interlayer s-wave SC [56–63].

In $La_4Ni_3O_{10}$, the trilayer structure adds further complexity to its electronic nature [30,64]. Under pressure, trilayer $La_4Ni_3O_{10}$ undergoes a structural transition to the tetragonal $I4/mmm$ phase [31]. Valence counting suggests an average electronic configuration of $Ni^{2.67+}$ ($3d^{7.33}$), assigning four electrons to the two E_g orbitals across the three Ni atoms in each trilayer unit. Without considering the interlayer hopping, interorbital hybridization, or correlation effects, the hole number per E_g orbital is approximately 0.33, placing the system in the overdoped regime, according to cuprate standards [65–68]. Unlike the bilayer case, both E_g orbitals act as itinerant carriers, and the three layers are not fully equivalent, raising the fundamental question: what is the nature of SC in trilayer $La_4Ni_3O_{10}$?

In this study, we develop a strongly correlated two E_g-orbital t-$J_\parallel$-$J_\perp$ model to explore the SC in trilayer $La_4Ni_3O_{10}$ under pressure. Employing slave-boson mean-field (SBMF) theory [65,66], we self-consistently estimate the ground-state order parameters and holon densities. The trilayer structure, combined with finite hybridization effect, leads to itinerant E_g orbital bands with effective hole densities in the overdoped regime. Our numerical simulations show that SC in this trilayer system is predominantly driven by the $3d_{z^2}$ orbital, manifesting as intralayer extended s-wave pairing in the outer layers, accompanied by interlayer pairing. In contrast,

*These authors contributed equally to this work.

†Contact author: yangfan_blg@bit.edu.cn

‡Contact author: wucongjun@westlake.edu.cn

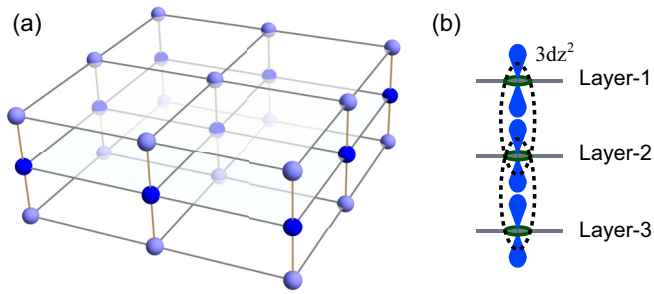

FIG. 1. (a) Trilayer lattice structure for the $La_3Ni_2O_7$. (b) Formation of the bonding bands in $3d_{z^2}$ orbital. The inner layer 2 could form bonding band with both the outer layer 1 and 3.

the $3d_{x^2-y^2}$ orbital exhibits much weaker pairing strength. We further explore the effect of doping to the $La_4Ni_3O_{10}$. Namely, we find that electron doping enhances SC, while hole doping suppresses it. Our results provide additional insights into the SC mechanism of trilayer $La_4Ni_3O_{10}$.

II. EFFECTIVE TRILAYER TWO-ORBITAL MODEL

The electronic characteristics of the trilayer $La_4Ni_3O_{10}$ under pressure are predominantly influenced by the two E_g orbitals within the NiO_2 planes. The trilayer configuration of the Ni ions is schematically shown in Fig. 1(a). Due to interlayer hopping, $3d_{z^2}$-orbital electrons residing on the inner layer can form bonding bands with those in both the upper and lower layers, as depicted in Fig. 1(b), which may be viewed as geometric frustration. Consequently, $3d_{z^2}$-orbital hole numbers within inner and outer layers would diverge. The electronic nature within inner and outer layers would be different. Experimentally, evidence points towards correlation effects, including observations of strange metal behavior in the normal state [27] and suppressed kinetic energy indicated by optical studies [46,52]. Furthermore, the local Hubbard interaction U on the Ni ions, largely insensitive to the specific lattice details, is estimated to be $U \approx 4-5$ eV (e.g., a similar value was used for $La_3Ni_2O_7$ in Ref. [12]), significantly exceeding the characteristic intersite hopping energy 0.7 eV. These points firmly place the system within the correlated regime, thereby motivating the development of a strong-coupling effective theory in the subsequent analysis.

The intralayer Hamiltonian $H_\parallel$ is given by

$$\begin{aligned} H_\parallel = &- \sum_{\langle i,j\rangle,\alpha,\sigma} (t_\parallel^{x\alpha} d^\dagger_{x\alpha\sigma}(i) d_{x\alpha\sigma}(j) + \text{H.c.}) \\ &- \sum_{\langle i,j\rangle,\alpha,\sigma} (t_\parallel^{z\alpha} d^\dagger_{z\alpha\sigma}(i) d_{z\alpha\sigma}(j) + \text{H.c.}) \\ &- \sum_{\langle i,j\rangle,\alpha,\sigma} t_{\parallel,j-i}^{xz\alpha} (d^\dagger_{x\alpha\sigma}(i) d_{z\alpha\sigma}(j) + \text{H.c.}) \\ &+ \sum_{\langle i,j\rangle,\alpha} [J_\parallel^{x\alpha} \boldsymbol{S}_{x\alpha}(i)\cdot\boldsymbol{S}_{x\alpha}(j) + J_\parallel^{z\alpha} \boldsymbol{S}_{z\alpha}(i)\cdot\boldsymbol{S}_{z\alpha}(j)], \end{aligned} \quad (1)$$

where $d^\dagger_{x\alpha\sigma}(i)/d^\dagger_{z\alpha\sigma}(i)$ creates a $3d_{x^2-y^2}/3d_{z^2}$-orbital electron with spin $\sigma = \uparrow, \downarrow$ at the lattice site i in the layer $\alpha = 1, 2, 3$. $\boldsymbol{S}_{x\alpha}(i) = \frac{1}{2} d^\dagger_{x\alpha\sigma}(i)[\boldsymbol{\sigma}]_{\sigma\sigma'} d_{x\alpha\sigma'}(i)$ is the spin operator for the $3d_{x^2-y^2}$ orbital, with Pauli matrix $\boldsymbol{\sigma} = (\sigma_x, \sigma_y, \sigma_z)$; similar for the $3d_{z^2}$-orbital spin $\boldsymbol{S}_{z\alpha}(i)$. $\langle ij\rangle$ represents the summation over all the intralayer nearest-neighbor (NN) bonds. $H_\parallel$ describes three intralayer t-$J_\parallel$ models of the two E_g orbitals, with the corresponding intralayer NN hopping terms $t_\parallel^{x\alpha}$ and $t_\parallel^{z\alpha}$, and antiferromagnetic (AFM) spin-exchange terms $J_\parallel^{x\alpha}$ and $J_\parallel^{z\alpha}$. $t_{\parallel,j-i}^{xz\alpha}$ represent the finite NN hybridization between the two E_g orbitals, which exhibit opposite signs along x and y directions due to the symmetry constraint $t_{\parallel,x}^{xz\alpha} = -t_{\parallel,y}^{xz\alpha}$. The hole densities within α layer are denoted as $\delta_{x\alpha}$ and $\delta_{z\alpha}$ for $3d_{x^2-y^2}$ and $3d_{z^2}$ orbitals, respectively.

The interactions among the three layers are facilitated by the interlayer hoppings of $3d_{z^2}$ orbitals and interlayer superexchanges. The three layers are categorized into two types, with the inner layer denoted by $\alpha = 2$ and the outer layers labeled as $\alpha = 1, 3$. The interlayer hoppings and exchanges are described by the following expressions:

$$\begin{aligned} H_\perp = &- \sum_{i,\sigma;\alpha=1,3} (t_\perp^z d^\dagger_{z2\sigma}(i) d_{z\alpha\sigma}(i) + \text{H.c.}) \\ &+ \sum_{i;\alpha=1,3} [J_\perp^x \boldsymbol{S}_{x2}(i)\cdot\boldsymbol{S}_{x\alpha}(i) + J_\perp^z \boldsymbol{S}_{z2}(i)\cdot\boldsymbol{S}_{z\alpha}(i)], \end{aligned} \quad (2)$$

involving the NN interlayer hoppings $t_\perp^z$ and AFM spin exchanges between the inner layer $\alpha = 2$ and the outer layers $\alpha = 1, 3$. The robust interlayer exchange $J_\perp^z$ arises from the NN interlayer hopping of the $3d_{z^2}$ orbital in the strong-coupling limit. Additionally, a finite superexchange $J_\perp^x$ associated with the $3d_{x^2-y^2}$ orbital is transmitted from the $3d_{z^2}$ orbital due to the robust Hund's rule coupling [56–61], as depicted in Fig. 1(b). It should be noted that this mechanism can only be realized when the $3d_{z^2}$ orbital is singly occupied, resulting in the effective renormalized $J_\perp^x$ by the filling of $3d_{z^2}$ orbital. A similar situation leads to a nonzero effective intralayer superexchange $J_\parallel^{z\alpha}$ for the $3d_{z^2}$ orbital, which is transmitted from the $3d_{x^2-y^2}$ orbital. A preliminary analysis yields the following leading-order approximations,

$$\begin{aligned} J_\parallel^{z1} &= J_\parallel^{z3} = J_\parallel (1-\delta_{x1})^2, \\ J_\parallel^{z2} &= J_\parallel (1-\delta_{x2})^2, \\ J_\perp^x &= J_\perp (1-\delta_{z1})(1-\delta_{z2}), \end{aligned} \quad (3)$$

where the effective exchanges are mostly generated when the intermediate orbitals are occupied. The larger holon densities would suppress these effective AFM spin exchanges.

We adopt the physical parameters of the hopping parameters from the DFT calculations with full structure relaxations [40]. The hopping parameters within the outer layers are given by $t_\parallel^{x1} = t_\parallel^{x3} = 0.532$ eV, $t_\parallel^{z1} = t_\parallel^{z3} = 0.1558$ eV, and $t_\parallel^{xz1} = t_\parallel^{xz3} = 0.282$ eV. For the inner layer, $t_\parallel^{x2} = 0.545$ eV, $t_\parallel^{z2} = 0.1373$ eV, and $t_\parallel^{xz2} = 0.2945$ eV. The robust interlayer hopping for the $3d_{z^2}$ orbital is $t_\perp^z = 0.7082$ eV, while the interlayer one for $3d_{x^2-y^2}$ nearly vanishes. The onsite energies are chosen as $E_{x1} = E_{x3} = 0.358$ eV, $E_{x2} = 0.656$ eV, $E_{z1} = E_{z3} = 0$ eV, and $E_{z2} = 0.42$ eV.

In the strong coupling limit, effective AFM spin exchanges can arise from the NN hoppings. We take the interlayer AFM strength for $3d_{z^2}$-orbital as $J_\perp^z \equiv J_\perp = 0.5$ eV, while the intralayer one for $3d_{z^2}$ orbital is $J_\parallel^x \equiv J_\parallel = 0.25$ eV. The

TABLE I. Table of the hopping and pairing order parameters (OPs) as well as the holon densities $\delta_{x\alpha}$ and $\delta_{z\alpha}$ calculated by the SBMF theory in the ground state (GS) for $J_\parallel = 0.25$ eV and $J_\perp/J_\parallel = 2$.

OP	GS value (eV)	OP	GS value (eV)
$\Delta_\perp^z$	-2.97×10^{-4}	$\chi_\perp^z$	1.17×10^{-1}
$\Delta_\perp^x$	-1.0×10^{-5}	$\chi_\perp^x$	1.22×10^{-3}
$\Delta_\parallel^{x2}$	4.37×10^{-5}	$\chi_\parallel^{x2}$	2.79×10^{-2}
$\Delta_\parallel^{z2}$	2.73×10^{-5}	$\chi_\parallel^{z2}$	4.07×10^{-4}
$\Delta_\parallel^{x1}$	4.33×10^{-5}	$\chi_\parallel^{x1}$	3.10×10^{-2}
$\Delta_\parallel^{z1}$	5.28×10^{-4}	$\chi_\parallel^{z1}$	1.32×10^{-3}
	Holon density		Holon density
δ_{x1}	0.402	δ_{z1}	0.171
δ_{x2}	0.523	δ_{z2}	0.332

transmitted interaction strengths $J_\perp^x$ and $J_\parallel^{z\alpha}$ depend on the occupied densities of the relevant orbitals.

The t-J-like model is appropriate for strongly correlated systems where double occupancy is prohibited; SBMF is particularly well suited for studying such models as its formalism naturally incorporates this constraint. In the SBMF theory [65,66], the electronic operators are expressed as a combination of spinon and holon part, i.e., $c_{i\sigma}^\dagger = f_{i\sigma}^\dagger h_i$. The spin-exchange interactions could be decomposed into spinon hopping and pairing channels, yielding the following mean-field expressions:

$$\begin{aligned}
\chi_\parallel^{s\alpha} &= \tfrac{3}{8} J_\parallel^{s\alpha} \langle f_{s\alpha\uparrow}^\dagger(j) f_{s\alpha\uparrow}(i) + f_{s\alpha\downarrow}^\dagger(j) f_{s\alpha\downarrow}(i)\rangle, \\
\Delta_\parallel^{s\alpha} &= \tfrac{3}{8} J_\parallel^{s\alpha} \langle f_{s\alpha\downarrow}(j) f_{s\alpha\uparrow}(i) - f_{s\alpha\uparrow}(j) f_{s\alpha\downarrow}(i)\rangle, \\
\chi_\perp^{s} &= \tfrac{3}{8} J_\perp^{s} \langle f_{s2\uparrow}^\dagger(i) f_{s1\uparrow}(i) + f_{s2\downarrow}^\dagger(i) f_{s1\downarrow}(i)\rangle, \\
\Delta_\perp^{s} &= \tfrac{3}{8} J_\perp^{s} \langle f_{s2\downarrow}(i) f_{s1\uparrow}(i) - f_{s2\uparrow}(i) f_{s1\downarrow}(i)\rangle,
\end{aligned} \tag{4}$$

with $s = x, z$ for the $3d_{x^2-y^2}$, $3d_{z^2}$ orbital, respectively. The strengths of the ground-state order parameters and holon densities are numerically solved, as summarized in Table I. In the relevant parameter regime $J_\parallel = 0.25$ eV and $J_\perp/J_\parallel = 2$, the holon densities for the $3d_{x^2-y^2}$ orbital fall within the overdoped regime, $\delta_{x1} = 0.402$ and $\delta_{x2} = 0.523$, resulting in a reduction in its intralayer pairing strengths. In contrast, $3d_{z^2}$-orbital holon densities are $\delta_{z1} = 0.171$ and $\delta_{z2} = 0.332$, with the outer-layer one δ_{z1} closely approaching the optimal doping level of cuprates. This property suggests the potential for achieving SC in this orbital.

III. SUPERCONDUCTIVITY

In the trilayer system, potential SC exhibits both intralayer and interlayer pairings for the two orbitals. Numerical simulated results for the $J_\parallel$ dependence of all the relevant spinon pairing strengths are presented in Fig. 2(a). Among the pairing channels, the interlayer pairing $\Delta_\perp^z$ and outer-layer one $\Delta_\parallel^{z1}$ for the $3d_{z^2}$ orbital exhibit the largest amplitudes, being the dominance within the relevant parameter regime. Here, the intralayer pairing exhibits the same phase along the x and y directions, leading to extended s-wave pairing. Interestingly, the interlayer and intralayer pairings exhibit opposite signs, as illustrated in Fig. 2(b). In a lateral view, the pairing character

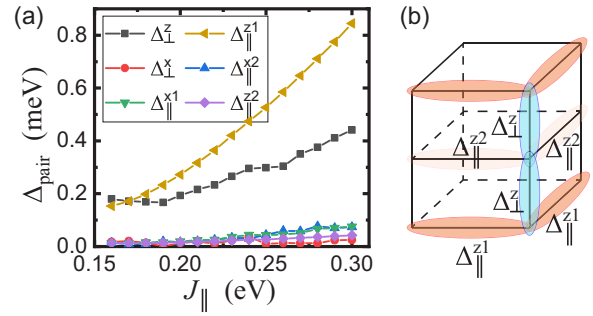

FIG. 2. (a) Spinon pairing strengths $|\Delta_{\rm pair}|$ versus exchange strengths $J_\parallel$ at fixed $J_\perp/J_\parallel = 2$. (b) Schematic diagram for the dominant $3d_{z^2}$-orbital trilayer pairing structure. The intralayer and interlayer pairings exhibit opposite signs.

reflects a d-wave-like nature, signifying a change in the sign of the superconducting pairing from the parallel (intralayer) to the perpendicular (interlayer) direction. The paring strengths in the $3d_{x^2-y^2}$ orbital are markedly suppressed owing to its overdoped nature.

The superconducting state is realized when spinons are paired and holons are condensed [65,66], characterized by the SC order parameter $\tilde{\Delta}_{\rm SC} = \delta\Delta_{\rm pair}$. The numerical results for the $J_\parallel$ dependence of the several SC pairing strengths are summarized in Fig. 3(a). The superconducting T_c is determined by the lower of the holon condensation temperature $T_{\rm BEC}$ and the spinon pairing temperature $T_{\rm pair}$. Holon condensation is effectively characterized by a generalized two-dimensional (2D) XY-like model, where $T_{\rm BEC}$ is replaced by the Kosterlitz–Thouless (KT) transition temperature [69], proportional to the superfluid stiffness $\rho_{s\alpha}$ within orbital s and layer α. The estimation of $\rho_{s\alpha}$ is given by

$$\rho_{s\alpha} = 2\delta_{s\alpha} t_\parallel^{s\alpha} \chi_\parallel^{s\alpha} / \left(\tfrac{3}{8} J_{s\parallel}^{\alpha}\right). \tag{5}$$

From the order parameters listed in Table I, we roughly estimate $T_{\rm BEC}^{s\alpha} = \frac{\pi}{2}\rho_{s\alpha}$ for the s orbital in the α layer: $T_{\rm BEC}^{x1} \approx 2.22 \times 10^{-1}$ eV, $T_{\rm BEC}^{x2} \approx 2.67 \times 10^{-1}$ eV, $T_{\rm BEC}^{z1} \approx 3.32 \times 10^{-3}$ eV, and $T_{\rm BEC}^{z2} \approx 2.72 \times 10^{-3}$ eV. Clearly, $3d_{x^2-y^2}$ orbital exhibits a much larger condensation temperature than $3d_{z^2}$ orbital, due to the larger holon densities.

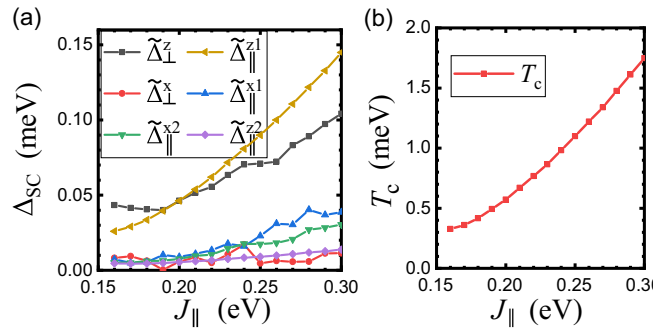

FIG. 3. (a) Superconducting pairing strengths $|\Delta_{\rm SC}|$ versus exchange strengths $J_\parallel$ with fixed $J_\perp/J_\parallel = 2$. $3d_{z^2}$-orbital interlayer pairing $\tilde{\Delta}_\perp^z$ and outer-extended s-wave pairing $\tilde{\Delta}_\parallel^{z1}$ dominate in the relevant parameter regime. (b) Superconducting T_c versus $J_\parallel$.

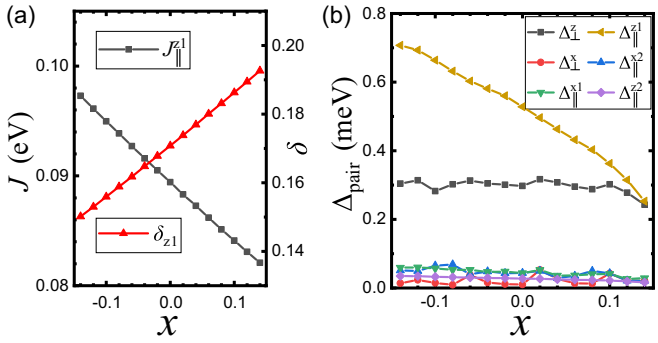

FIG. 4. (a) Outer-layer effective superexchanges $J_\parallel^{z1}$ and holon densities δ_{z1} versus dopings x, with $x > 0$ for hole dopings and $x < 0$ for electron dopings. (b) Spinon pairings versus dopings x. $3d_{z^2}$ orbital interlayer pairing $\Delta_\perp^z$ nearly maintains the same amplitude under doping.

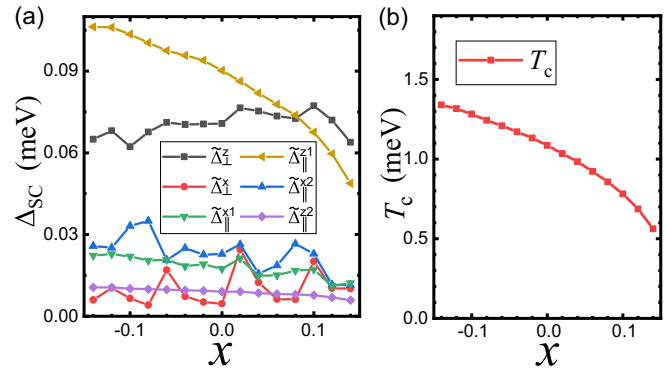

FIG. 5. (a) Superconducting pairing order parameters versus dopings x. (b) Superconducting T_c versus dopings x. T_c increases under electron doping and reduces under hole doping.

Owing to the overdoped nature of the two orbitals, T_c is governed by the spinon pairing temperature T_{pair}, which is lower than the condensation T_{BEC}. The dependence of superconducting T_c on the spin exchange $J_\parallel$ with fixed $J_\perp/J_\parallel = 2$ is depicted in Fig. 3(b), exhibiting a qualitatively similar trend to the ground-state pairing strength $\tilde{\Delta}_\parallel^{z1}$. In the presence of higher interaction strengths, T_c naturally becomes larger with increasing $J_\parallel$.

The ground-state order parameters reveal clear signatures of orbital-selective doping and correlation effects, highlighting the potential for SC to emerge predominantly in the d_{z^2} orbital. Prior studies based on SBMF theory for the single-layer t-J model have demonstrated that the spinon pairing temperature decreases with increasing doping, eventually becoming strongly suppressed in the heavily overdoped regime around $\delta \approx 0.3 \sim 0.4$ [65]. This theoretical trend aligns well with experimental observations in cuprates, where SC weakens beyond optimal doping [65–68].

Here, the numerical results for trilayer $La_4Ni_3O_{10}$ exhibit a consistent pattern. For the $d_{x^2-y^2}$ orbital, the hole concentration lies in the range of $\delta \approx 0.4 \sim 0.5$, placing it deep in the overdoped regime. As a result, the pairing amplitude is significantly suppressed, and the corresponding spinon pairing temperature is very low. In contrast, the d_{z^2} orbital remains less doped, with $\delta_{z1} = 0.171$ for the outer layer and $\delta_{z2} = 0.332$ for the inner layer. These lower doping levels support a stronger pairing amplitude and lead to a much higher pairing temperature relative to the $d_{x^2-y^2}$ orbital.

IV. EFFECTS OF DOPING

The doping dependence of the trilayer system is systematically investigated in Fig. 4, when the average number of electrons per unit cell is $4 - x$ with doping fraction x. Here, $x < 0$ corresponds to electron doping, while $x > 0$ corresponds to hole doping. As the doping x varies from -0.1 to 0.1, the effective outer-layer $3d_{z^2}$-orbital holon density increases, as illustrated in Fig. 4(a). This is accompanied by a decrease in the effective coupling $J_\parallel^{z1}$, leading to a suppression in the outer-layer spinon pairing $\Delta_\parallel^{z1}$ [65]. The simulated pairing strength $\Delta_\parallel^{z1}$ clearly exhibits an increase under electron doping and a reduction under hole doping, as depicted in Fig. 4(b). The interlayer pairings $\Delta_\perp^z$ of the $3d_{z^2}$ orbital maintain nearly the same amplitudes as x varies.

The evolution of the SC order parameters under doping is further verified in Fig. 5(a). The interlayer pairing and outer-layer pairing of the $3d_{z^2}$ orbital dominate. Specifically, $\tilde{\Delta}_\parallel^{z1}$ is suppressed as x increases. The superconducting T_c increase under the electron doping ($x < 0$) and decrease under hole doping ($x > 0$), as shown in Fig. 5(b), following a similar tendency as the $\tilde{\Delta}_\parallel^{z1}$.

V. COMPARISON BETWEEN TRILAYER AND BILAYER SYSTEM

The superconducting behaviors in $La_4Ni_3O_{10}$ and $La_3Ni_2O_7$ diverge due to differences in the E_g-orbital filling factor and multilayer structure. In $La_3Ni_2O_7$, the bilayer configuration leads to a robust bonding band of $3d_{z^2}$ orbital, which is nearly fully occupied and localized [56,57]. Consequently, the $3d_{x^2-y^2}$ orbital acts as the source of mobile carriers and exhibits a preference for strong interlayer pairing. Conversely, bands reconstruction of E_g orbitals in trilayer $La_4Ni_3O_{10}$ is reduced. As the $3d_{z^2}$ orbital is no longer close to half filling, the effective coupling $J_\perp^x$ is weakened, as indicated in Eq. (3), leading to a significant reduction in interlayer $3d_{x^2-y^2}$-orbital exchange.

The spinon Fermi surface (FS) in Fig. 6 further elucidates this distinction, where the color-coded compositions of the inner and outer layers are depicted. The outer-layer $3d_{z^2}$ orbital dominates in most of the regime, while the contribution from the inner-layer $3d_{z^2}$ orbital is minimal. The low density of the inner-layer $3d_{z^2}$ orbital near the FS in $La_4Ni_3O_{10}$ strongly hinders the interlayer pairing of the $3d_{z^2}$ orbital compared to $La_3Ni_2O_7$. Moreover, the $3d_{z^2}$-orbital holon density in the outer layer is approximately 0.17, close to the optimal hole-doping level. However, the intralayer superexchange interaction for $3d_{z^2}$ electrons is also weak, rendering intralayer pairing fragile and susceptible to destruction by thermal fluctuations. As a result, the superconducting behavior is predominantly characterized by intralayer extended s-wave pairing in the outer layers combined with interlayer pairing within $3d_{z^2}$ orbital. Moreover, the pairing frustration

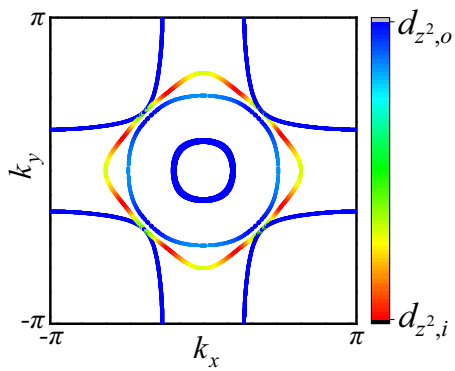

FIG. 6. The spinon Fermi surface. The right-side color panel shows the various components with the red and blue colors representing the inner-layer $3d_{z^2}$ and the outer-layer $3d_{z^2}$ orbitals, respectively.

induced by the trilayer structure and higher holon densities in $3d_{z^2}$ orbital in pressurized $La_4Ni_3O_{10}$ lead to a significantly lower T_c compared to pressurized $La_3Ni_2O_7$.

The differences between our calculated spinon FS and ARPES measurements [28,47,64] likely stem from the simplifications in our tight-binding model, which deliberately excludes longer-range hopping and certain interactions to focus on dominant correlation effects. While including these additional terms could refine quantitative details like FS curvature and nesting features, we do not expect them to qualitatively alter the fundamental pairing symmetry or mechanism identified here.

VI. DISCUSSION

In summary, our investigation reveals that the $3d_{z^2}$ orbital primarily drives the superconducting behavior in the trilayer compound $La_4Ni_3O_{10}$, while $3d_{x^2-y^2}$ orbital plays an important role as a hidden bridge. An intralayer extended s-wave pairing within the outer layers, accompanied by an interlayer pairing with opposite sign, is stabilized in the numerical simulation, which exhibits a d-wave configuration in the side view. The numerical simulation further predicts that electron doping could enhance the pairing strength and critical temperature.

It is important to note, however, that the T_c values calculated in our study are somewhat lower than those observed experimentally [26–28]. This discrepancy can be primarily attributed to two main simplifications in our minimal model. First, by focusing on the most relevant degrees of freedom, our model neglects long-range hopping processes and additional interactions that could potentially enhance T_c. Secondly, the SBMF approximation neglects certain quantum and thermal fluctuations which can play a significant role in strongly correlated systems and influence the transition temperature. Despite these limitations, our approach captures the proposed pairing mechanism's qualitative features, including its orbital selectivity and doping dependence, thus providing valuable insights despite the difference in absolute T_c values.

The discovery of superconductivity in pressurized $La_{n+1}Ni_nO_{3n+1}$ for $n = 2$ and $n = 3$ naturally raises the question of the optimal layer number, n, for SC within this nickelates series. Current experimental evidence indicates that $n = 2$ already represents the optimal layered structure for these materials, in contrast to multilayer cuprates, where $n = 3$ or $n = 4$ is considered optimal for SC [70]. This divergence may be attributed to differences in the underlying electronic structures: Nickelates $La_{n+1}Ni_nO_{3n+1}$ series have two E_g orbitals near the Fermi level, while cuprates exhibit a single $3d_{x^2-y^2}$ orbital. Additionally, the $3d_{z^2}$ orbital in $La_{n+1}Ni_nO_{3n+1}$ facilitates strong interlayer hopping, resulting in robust interlayer superexchange, whereas cuprates only exhibit weak interlayer Josephson coupling [71,72]. Furthermore, the multiorbital nature and the role of Hundness [59–61,73,74] in generating strong correlations in nickelates may play a pivotal role in their superconductivity. A comprehensive understanding of the complex nature of superconductivity in this class of materials requires further theoretical and numerical investigations.

ACKNOWLEDGMENTS

We are grateful to the stimulating discussions with Wei Li. C.W. is supported by the National Natural Science Foundation of China under the Grants No. 12234016 and No. 12174317. F.Y. is supported by the National Natural Science Foundation of China under the Grant No. 12074031. C.L. is supported by the National Natural Science Foundation of China under the Grant No. 12304180. This work has been supported by the New Cornerstone Science Foundation.

DATA AVAILABILITY

The data that support the findings of this article are not publicly available. The data are available from the authors upon reasonable request.

[1] S. Taniguchi, T. Nishikawa, Y. Yasui, Y. Kobayashi, J. Takeda, S.-i. Shamoto, and M. Sato, Transport, magnetic and thermal properties of $La_3Ni_2O_{7-\delta}$, J. Phys. Soc. Jpn. **64**, 1644 (1995).

[2] D.-K. Seo, W. Liang, M.-H. Whangbo, Z. Zhang, and M. Greenblatt, Electronic band structure and madelung potential study of the nickelates La_2NiO_4,$La_3Ni_2O_7$, and $La_4Ni_3O_{10}$, Inorg. Chem. **35**, 6396 (1996).

[3] Y. Kobayashi, S. Taniguchi, M. Kasai, M. Sato, T. Nishioka, and M. Kontani, Transport and magnetic properties of $La_3Ni_2O_{7-\delta}$ and $La_4Ni_3O_{10-\delta}$, J. Phys. Soc. Jpn. **65**, 3978 (1996).

[4] M. Greenblatt, Ruddlesden-popper $Ln_{n+1}Ni_nO_{3n+1}$ nickelates: structure and properties, Curr. Opin. Solid State Mater. Sci. **2**, 174 (1997).

[5] M. Greenblatt, Z. Zhang, and M. Whangbo, Electronic properties of $La_3Ni_2O_7$ and $Ln_4Ni_3O_{10}$, Ln= La, Pr and Nd, Synth. Met. **85**, 1451 (1997).

[6] C. D. Ling, D. N. Argyriou, G. Wu, and J. Neumeier, Neutron diffraction study of $La_3Ni_2O_7$: Structural relationships among n =1,2, and 3 phases $La_{n+1}Ni_nO_{3n+1}$, J. Solid State Chem. **152**, 517 (2000).

[7] G. Wu, J. J. Neumeier, and M. F. Hundley, Magnetic susceptibility, heat capacity, and pressure dependence of the electrical resistivity of $La_3Ni_2O_7$ and $La_4Ni_3O_{10}$, Phys. Rev. B **63**, 245120 (2001).

[8] T. Fukamachi, Y. Kobayashi, T. Miyashita, and M. Sato, ^{139} La NMR studies of layered perovskite systems $La_3Ni_2O_{7-\delta}$ and $La_4Ni_3O_{10}$, J. Phys. Chem. Solids **62**, 195 (2001).

[9] V. I. Voronin, I. F. Berger, V. A. Cherepanov, L. Y. Gavrilova, A. N. Petrov, A. I. Ancharov, B. Tolochko, and S. G. Nikitenko, Neutron diffraction, synchrotron radiation and exafs spectroscopy study of crystal structure peculiarities of the lanthanum nickelates $La_{n+1}Ni_nO_y$ ($n = 1, 2, 3$), Nucl. Instrum. Methods Phys. Res., Sect. A **470**, 202 (2001).

[10] D. O. Bannikov, A. P. Safronov, and V. A. Cherepanov, Thermochemical characteristics of $La_{n+1}Ni_nO_{3n+1}$ oxides, Thermochim. Acta **451**, 22 (2006).

[11] T. Hosoya, K. Igawa, Y. Takeuchi, K. Yoshida, T. Uryu, H. Hirabayashi, and H. Takahashi, Pressure studies on the electrical properties in $R_{2-x}Sr_xNi_{1-y}Cu_yO_{4+\delta}$ (R=La, Nd) and $La_3Ni_2O_{7+\delta}$, J. Phys.: Conf. Ser. **121**, 052013 (2008).

[12] V. Pardo and W. E. Pickett, Metal-insulator transition in layered nickelates $La_3Ni_2O_{7-\delta}$ ($\delta = 0.0, 0.5, 1$), Phys. Rev. B **83**, 245128 (2011).

[13] M. Nakata, D. Ogura, H. Usui, and K. Kuroki, Finite-energy spin fluctuations as a pairing glue in systems with coexisting electron and hole bands, Phys. Rev. B **95**, 214509 (2017).

[14] Y. Mochizuki, H. Akamatsu, Y. Kumagai, and F. Oba, Strain-engineered peierls instability in layered perovskite $La_3Ni_2O_7$ from first principles, Phys. Rev. Mater. **2**, 125001 (2018).

[15] Z. Li, W. Guo, T. T. Zhang, J. H. Song, T. Y. Gao, Z. B. Gu, and Y. F. Nie, Epitaxial growth and electronic structure of ruddlesden–popper nickelates ($La_{n+1}Ni_nO_{3n+1}$, $n = 1$–5), APL Mater. **8**, 091112 (2020).

[16] J. Song, D. Ning, B. Boukamp, J.-M. Bassat, and H. J. Bouwmeester, Structure, electrical conductivity and oxygen transport properties of Ruddlesden-Popper phases $Ln_{n+1}Ni_nO_{3n+1}$ (Ln=La, Pr and Nd; n=1, 2 and 3), J. Mater. Chem. A **8**, 22206 (2020).

[17] M. R. Barone, N. M. Dawley, H. P. Nair, B. H. Goodge, M. E. Holtz, A. Soukiassian, E. E. Fleck, K. Lee, Y. Jia, T. Heeg, R. Gatt, Y. Nie, D. A. Muller, L. F. Kourkoutis, and D. G. Schlom, Improved control of atomic layering in perovskite-related homologous series, APL Mater. **9**, 021118 (2021).

[18] Z. Liu, H. Sun, M. Huo, X. Ma, Y. Ji, E. Yi, L. Li, H. Liu, J. Yu, Z. Zhang, Z. Chen, F. Liang, H. Dong, H. Guo, D. Zhong, B. Shen, S. Li, and M. Wang, Evidence for charge and spin density waves in single crystals of $La_3Ni_2O_7$ and $La_3Ni_2O_6$, Sci. China Phys. Mech. Astron. **66**, 217411 (2023).

[19] D. Li, K. Lee, B. Y. Wang, M. Osada, S. Crossley, H. R. Lee, Y. Cui, Y. Hikita, and H. Y. Hwang, Superconductivity in an infinite-layer nickelate, Nature (London) **572**, 624 (2019).

[20] H. Sun, M. Huo, X. Hu, J. Li, Z. Liu, Y. Han, L. Tang, Z. Mao, P. Yang, B. Wang *et al.*, Signatures of superconductivity near 80k in a nickelate under high pressure, Nature (London) **621**, 493 (2023).

[21] J. Hou, P.-T. Yang, Z.-Y. Liu, J.-Y. Li, P.-F. Shan, L. Ma, G. Wang, N.-N. Wang, H.-Z. Guo, J.-P. Sun, Y. Uwatoko, M. Wang, G.-M. Zhang, B.-S. Wang, and J.-G. Cheng, Emergence of high-temperature superconducting phase in pressurized $La_3Ni_2O_7$ crystals, Chin. Phys. Lett. **40**, 117302 (2023).

[22] Y. Zhang, D. Su, Y. Huang, Z. Shan, H. Sun, M. Huo, K. Ye, J. Zhang, Z. Yang, Y. Xu, Y. Su, R. Li, M. Smidman, M. Wang, L. Jiao, and H. Yuan, High-temperature superconductivity with zero resistance and strange-metal behaviour in $La_3Ni_2O_{7-\delta}$, Nat. Phys. **20**, 1269 (2024).

[23] G. Wang, N. N. Wang, X. L. Shen, J. Hou, L. Ma, L. F. Shi, Z. A. Ren, Y. D. Gu, H. M. Ma, P. T. Yang, Z. Y. Liu, H. Z. Guo, J. P. Sun, G. M. Zhang, S. Calder, J.-Q. Yan, B. S. Wang, Y. Uwatoko, and J.-G. Cheng, Pressure-induced superconductivity in polycrystalline $La_3Ni_2O_{7-\delta}$, Phys. Rev. X **14**, 011040 (2024).

[24] G. Wang, N. Wang, Y. Wang, L. Shi, X. Shen, J. Hou, H. Ma, P. Yang, Z. Liu, H. Zhang, X. Dong, J. Sun, B. Wang, K. Jiang, J. Hu, Y. Uwatoko, and J. Cheng, Observation of high-temperature superconductivity in the high-pressure tetragonal phase of $La_2PrNi_2O_{7-\delta}$, arXiv:2311.08212.

[25] E. K. Ko, Y. Yu, Y. Liu, L. Bhatt, J. Li, V. Thampy, C.-T. Kuo, B. Y. Wang, Y. Lee, K. Lee *et al.*, Signatures of ambient pressure superconductivity in thin film $La_3Ni_2O_7$, Nature (London) **638**, 935 (2025).

[26] Q. Li, Y.-J. Zhang, Z.-N. Xiang, Y. Zhang, X. Zhu, and H.-H. Wen, Signature of superconductivity in pressurized $La_4Ni_3O_{10}$, Chin. Phys. Lett. **41**, 017401 (2024).

[27] Y. Zhu, D. Peng, E. Zhang, B. Pan, X. Chen, L. Chen, H. Ren, F. Liu, Y. Hao, N. Li *et al.*, Superconductivity in pressurized trilayer $La_4Ni_3O_{10-\delta}$ single crystals, Nature (London) **631**, 531 (2024).

[28] M. Zhang, C. Pei, D. Peng, X. Du, W. Hu, Y. Cao, Q. Wang, J. Wu, Y. Li, H. Liu, C. Wen, J. Song, Y. Zhao, C. Li, W. Cao, S. Zhu, Q. Zhang, N. Yu, P. Cheng, L. Zhang, Z. Li, J. Zhao, Y. Chen, C. Jin, H. Guo, C. Wu, F. Yang, Q. Zeng, S. Yan, L. Yang, and Y. Qi, Superconductivity in trilayer nickelate $La_4Ni_3O_{10}$ under pressure, Phys. Rev. X **15**, 021005 (2025).

[29] N. Yuan, A. Elghandour, J. Arneth, K. Dey, and R. Klingeler, High-pressure crystal growth and investigation of the metal-to-metal transition of Ruddlesden-Popper trilayer nickelates $La_4Ni_3O_{10}$, J. Cryst. Growth **627**, 127511 (2024).

[30] H. Sakakibara, M. Ochi, H. Nagata, Y. Ueki, H. Sakurai, R. Matsumoto, K. Terashima, K. Hirose, H. Ohta, M. Kato, Y. Takano, and K. Kuroki, Theoretical analysis on the possibility of superconductivity in the trilayer Ruddlesden-Popper nickelate $La_4Ni_3O_{10}$ under pressure and its experimental examination: Comparison with $La_3Ni_2O_7$, Phys. Rev. B **109**, 144511 (2024).

[31] J. Li, C.-Q. Chen, C. Huang, Y. Han, M. Huo, X. Huang, P. Ma, Z. Qiu, J. Chen, X. Hu, L. Chen, T. Xie, B. Shen, H. Sun, D. Yao, and M. Wang, Structural transition, electric transport, and electronic structures in the compressed trilayer nickelate $La_4Ni_3O_{10}$, Sci. China Phys. Mech. Astron. **67**, 117403 (2024).

[32] M. Kakoi, T. Oi, Y. Ohshita, M. Yashima, K. Kuroki, T. Kato, H. Takahashi, S. Ishiwata, Y. Adachi, N. Hatada, T. Uda, and H. Mukuda, Multiband metallic ground state in multilayered nickelates $La_3Ni_2O_7$ and $La_4Ni_3O_{10}$ probed by ^{139}la-nmr at ambient pressure, J. Phys. Soc. Jpn. **93**, 053702 (2024).

[33] I. V. Leonov, Electronic structure and magnetic correlations in the trilayer nickelate superconductor $La_4Ni_3O_{10}$ under pressure, Phys. Rev. B **109**, 235123 (2024).

[34] P.-F. Tian, H.-T. Ma, X. Ming, X.-J. Zheng, and H. Li, Effective model and electron correlations in trilayer nickelate superconductor $La_4Ni_3O_{10}$, J. Phys.: Condens. Matter **36**, 355602 (2024).

[35] J.-X. Wang, Z. Ouyang, R.-Q. He, and Z.-Y. Lu, Non-Fermi liquid and Hund correlation in $La_4Ni_3O_{10}$ under high pressure, Phys. Rev. B **109**, 165140 (2024).

[36] H. LaBollita, J. Kapeghian, M. R. Norman, and A. S. Botana, Electronic structure and magnetic tendencies of trilayer $La_4Ni_3O_{10}$ under pressure: Structural transition, molecular orbitals, and layer differentiation, Phys. Rev. B **109**, 195151 (2024).

[37] Y. Zhang, L.-F. Lin, A. Moreo, T. A. Maier, and E. Dagotto, Prediction of $s^{\pm}$-wave superconductivity enhanced by electronic doping in trilayer nickelates $La_4Ni_3O_{10}$ under pressure, Phys. Rev. Lett. **133**, 136001 (2024).

[38] Q.-G. Yang, K.-Y. Jiang, D. Wang, H.-Y. Lu, and Q.-H. Wang, Effective model and $s_{\pm}$-wave superconductivity in trilayer nickelate $La_4Ni_3O_{10}$, Phys. Rev. B **109**, L220506 (2024).

[39] C.-Q. Chen, Z. Luo, M. Wang, W. Wú, and D.-X. Yao, Trilayer multiorbital models of $La_4Ni_3O_{10}$, Phys. Rev. B **110**, 014503 (2024).

[40] M. Zhang, H. Sun, Y.-B. Liu, Q. Liu, W.-Q. Chen, and F. Yang, $s^{\pm}$-wave superconductivity in pressurized $La_4Ni_3O_{10}$, Phys. Rev. B **110**, L180501 (2024).

[41] Y. Li, Y. Cao, L. Liu, P. Peng, H. Lin, C. Pei, M. Zhang, H. Wu, X. Du, W. Zhao, K. Zhai, X. Zhang, J. Zhao, M. Lin, P. Tan, Y. Qi, G. Li, H. Guo, L. Yang, and L. Yang, Distinct ultrafast dynamics of bilayer and trilayer nickelate superconductors regarding the density-wave-like transitions, Sci. Bull. **70**, 180 (2025).

[42] F. Lechermann, S. Bötzel, and I. M. Eremin, Electronic instability, layer selectivity, and Fermi arcs in $La_3Ni_2O_7$, Phys. Rev. Mater. **8**, 074802 (2024).

[43] J. Huang and T. Zhou, Interlayer pairing-induced partially gapped Fermi surface in trilayer $La_4Ni_3O_{10}$ superconductors, Phys. Rev. B **110**, L060506 (2024).

[44] H. Oh, B. Zhou, and Y.-H. Zhang, Type II t-J model in charge transfer regime in bilayer $La_3Ni_2O_7$ and trilayer $La_4Ni_3O_{10}$, Phys. Rev. B **111**, L020504 (2025).

[45] Q. Qin, J. Wang, and Y. feng Yang, Frustrated superconductivity and intrinsic reduction of t_c in trilayer nickelate, Innovation Materials **2**, 100102 (2024).

[46] S. Xu, C.-Q. Chen, M. Huo, D. Hu, H. Wang, Q. Wu, R. Li, D. Wu, M. Wang, D.-X. Yao *et al.*, Origin of the density wave instability in trilayer nickelate $La_4Ni_3O_{10}$ revealed by optical and ultrafast spectroscopy, Phys. Rev. B **111**, 075140 (2025).

[47] X. Du, Y. Li, Y. Cao, C. Pei, M. Zhang, W. Zhao, K. Zhai, R. Xu, Z. Liu, Z. Li *et al.*, Correlated electronic structure and density-wave gap in trilayer nickelate $La_4Ni_3O_{10}$, arXiv:2405.19853.

[48] Z. Huo, P. Zhang, Z. Zhang, D. Duan, and T. Cui, Electronic correlations and Hund's rule coupling in trilayer nickelate $La_4Ni_3O_{10}$, arXiv:2407.00327.

[49] Y.-f. Yang, Decomposition of multilayer superconductivity with interlayer pairing, Phys. Rev. B **110**, 104507 (2024).

[50] Y. Zhang, L.-F. Lin, A. Moreo, T. A. Maier, and E. Dagotto, Magnetic correlations and pairing tendencies of the hybrid stacking nickelate superlattice $La_7Ni_5O_{17}$ ($La_3Ni_2O_7$/$La_4Ni_3O_{10}$) under pressure, arXiv:2408.07690.

[51] X. Huang, H. Zhang, J. Li, M. Huo, J. Chen, Z. Qiu, P. Ma, C. Huang, H. Sun, and M. Wang, Signature of superconductivity in pressurized trilayer-nickelate $Pr_4Ni_3O_{10-\delta}$, Chin. Phys. Lett. **41**, 127403 (2024).

[52] Z. Liu, J. Li, M. Huo, B. Ji, J. Hao, Y. Dai, M. Ou, Q. Li, H. Sun, B. Xu, Y. Lu, M. Wang, and H.-H. Wen, Evolution of electronic correlations in the Ruddlesden-Popper nickelates, arXiv:2411.08539.

[53] S. Deswal, D. Kumar, D. Rout, S. Singh, and P. Kumar, Dynamics of electron-electron correlated to electron-phonon coupled phase progression in trilayer nickelate $La_4Ni_3O_{10}$, arXiv:2411.13933.

[54] Y.-F. Zhao and A. S. Botana, Electronic structure of ruddlesden-popper nickelates: strain to mimic the effects of pressure, Phys. Rev. B **111**, 115154 (2025).

[55] Z. Luo, X. Hu, M. Wang, W. Wú, and D.-X. Yao, Bilayer two-orbital model of $La_3Ni_2O_7$ under pressure, Phys. Rev. Lett. **131**, 126001 (2023).

[56] C. Lu, Z. Pan, F. Yang, and C. Wu, Interlayer-coupling-driven high-temperature superconductivity in $La_3Ni_2O_7$ under pressure, Phys. Rev. Lett. **132**, 146002 (2024).

[57] C. Lu, Z. Pan, F. Yang, and C. Wu, Interplay of two E_g orbitals in superconducting $La_3Ni_2O_7$ under pressure, Phys. Rev. B **110**, 094509 (2024).

[58] H. Oh and Y.-H. Zhang, Type-ii t-J model and shared superexchange coupling from Hund's rule in superconducting $La_3Ni_2O_7$, Phys. Rev. B **108**, 174511 (2023).

[59] Y.-H. Tian, Y. Chen, J.-M. Wang, R.-Q. He, and Z.-Y. Lu, Correlation effects and concomitant two-orbital $s_{\pm}$-wave superconductivity in $La_3Ni_2O_7$ under high pressure, Phys. Rev. B **109**, 165154 (2024).

[60] X.-Z. Qu, D.-W. Qu, W. Li, and G. Su, Roles of Hund's rule and hybridization in the two-orbital model for high-T_c superconductivity in the bilayer nickelate, arXiv:2311.12769.

[61] M. Kakoi, T. Kaneko, H. Sakakibara, M. Ochi, and K. Kuroki, Pair correlations of the hybridized orbitals in a ladder model for the bilayer nickelate $La_3Ni_2O_7$, Phys. Rev. B **109**, L201124 (2024).

[62] X.-Z. Qu, D.-W. Qu, J. Chen, C. Wu, F. Yang, W. Li, and G. Su, Bilayer t-J-$J_{\perp}$ model and magnetically mediated pairing in the pressurized nickelate $La_3Ni_2O_7$, Phys. Rev. Lett. **132**, 036502 (2024).

[63] J. Chen, F. Yang, and W. Li, Orbital-selective superconductivity in the pressurized bilayer nickelate $La_3Ni_2O_7$: An infinite projected entangled-pair state study, Phys. Rev. B **110**, L041111 (2024).

[64] H. Li, X. Zhou, T. Nummy, J. Zhang, V. Pardo, W. E. Pickett, J. F. Mitchell, and D. S. Dessau, Fermiology and electron dynamics of trilayer nickelate la4ni3o10, Nat. Commun. **8**, 704 (2017).

[65] G. Kotliar and J. Liu, Superexchange mechanism and d-wave superconductivity, Phys. Rev. B **38**, 5142 (1988).

[66] P. A. Lee, N. Nagaosa, and X.-G. Wen, Doping a Mott insulator: Physics of high-temperature superconductivity, Rev. Mod. Phys. **78**, 17 (2006).

[67] B. Keimer, S. A. Kivelson, M. R. Norman, S. Uchida, and J. Zaanen, From quantum matter to high-temperature superconductivity in copper oxides, Nature (London) **518**, 179 (2015).

[68] C. Proust and L. Taillefer, The remarkable underlying ground states of cuprate superconductors, Annu. Rev. Condens. Matter Phys. **10**, 409 (2019).

[69] J. Kosterlitz and D. Thouless, Ordering, metastability and phase transitions in two-dimensional systems, J. Phys. C: Solid State Phys. **6**, 1181 (1973).

[70] A. Iyo, Y. Tanaka, H. Kito, Y. Kodama, P. M. Shirage, D. D. Shivagan, H. Matsuhata, K. Tokiwa, and T. Watanabe, t_c vs n relationship for multilayered high-t_c superconductors, J. Phys. Soc. Jpn. **76**, 094711 (2007).

[71] M. U. Ubbens and P. A. Lee, Spin-gap formation in bilayer cuprates due to enhanced interlayer pairing, Phys. Rev. B **50**, 438 (1994).

[72] K. Kuboki and P. A. Lee, Energy gap structure in bilayer oxide superconductors, J. Phys. Soc. Jpn. **64**, 3179 (1995).

[73] A. Georges, L. d. Medici, and J. Mravlje, Strong correlations from Hund's coupling, Annu. Rev. Condens. Matter Phys. **4**, 137 (2013).

[74] Z. Ouyang, J.-M. Wang, J.-X. Wang, R.-Q. He, L. Huang, and Z.-Y. Lu, Hund electronic correlation in $La_3Ni_2O_7$ under high pressure, Phys. Rev. B **109**, 115114 (2024).